Oncogenic fusion protein EWS-FLI1 is a network hub that regulates alternative splicing

Saravana P. Selvanathan[a], Garrett T. Graham[a], Hayriye V. Erkizan[a], Uta Dirksen[b], Thanemozhi G. Natarajan[c], Aleksandra Dakic[d], Songtao Yu[d], Xuefeng Liu[d], Michelle T. Paulsen[e], Mats E. Ljungman[e], Cathy H. Wu[c], Elizabeth R. Lawlor[f], Aykut Üren[a], and Jeffrey A. Toretsky[a,1]

[a]Department of Oncology and Pediatrics, Georgetown University, Washington, DC 20057; [b]Department of Pediatric Hematology and Oncology, University Hospital Münster, Westfalian Wilhelms University Münster, 48149 Münster, Germany; [c]Protein Information Resource, Georgetown University and University of Delaware, Washington, DC 20057; [d]Department of Pathology, Center for Cell Reprogramming, Georgetown University, Washington, DC 20057; and [e]Department of Radiation Oncology and Translational Oncology Program and [f]Departments of Pediatrics and Pathology, University of Michigan, Ann Arbor, Michigan, MI 48109

Edited by James L. Manley, Columbia University, New York, NY, and approved February 11, 2015 (received for review January 12, 2015)

The synthesis and processing of mRNA, from transcription to translation initiation, often requires splicing of intragenic material. The final mRNA composition varies based on proteins that modulate splice site selection. EWS-FLI1 is an Ewing sarcoma (ES) oncoprotein with an interactome that we demonstrate to have multiple partners in spliceosomal complexes. We evaluate the effect of EWS-FLI1 on posttranscriptional gene regulation using both exon array and RNA-seq. Genes that potentially regulate oncogenesis, including *CLK1*, *CASP3*, *PPFIBP1*, and *TERT*, validate as alternatively spliced by EWS-FLI1. In a CLIP-seq experiment, we find that EWS-FLI1 RNA-binding motifs most frequently occur adjacent to intron–exon boundaries. EWS-FLI1 also alters splicing by directly binding to known splicing factors including DDX5, hnRNP K, and PRPF6. Reduction of EWS-FLI1 produces an isoform of γ-TERT that has increased telomerase activity compared with wild-type (WT) TERT. The small molecule YK-4–279 is an inhibitor of EWS-FLI1 oncogenic function that disrupts specific protein interactions, including helicases DDX5 and RNA helicase A (RHA) that alters RNA-splicing ratios. As such, YK-4–279 validates the splicing mechanism of EWS-FLI1, showing alternatively spliced gene patterns that significantly overlap with EWS-FLI1 reduction and WT human mesenchymal stem cells (hMSC). Exon array analysis of 75 ES patient samples shows similar isoform expression patterns to cell line models expressing EWS-FLI1, supporting the clinical relevance of our findings. These experiments establish systemic alternative splicing as an oncogenic process modulated by EWS-FLI1. EWS-FLI1 modulation of mRNA splicing may provide insight into the contribution of splicing toward oncogenesis, and, reciprocally, EWS-FLI1 interactions with splicing proteins may inform the splicing code.

alternative splicing | EWS-FLI1 | TERT | Ewing sarcoma | CLK1

The alternative splicing of mRNA expands the diversity of the human proteome through evolution and ontogeny (1, 2). Spliceosomal network interactions, including proteins that recognize splice enhancer and silencer regions, are critical for the regulation of alternative splicing leading to protein isoforms with disparate functionality (3). Alternative splicing provides both a method by which to categorize subsets of cancers and an avenue for more effective targeted treatments (4). However, the spliceosomal protein interaction networks that are specific to cancer have not been systematically defined; alternative splicing can also change protein–protein interactions within networks (5). A systems biology approach can be used to study the relationship between splicing and oncogenesis by using tumor models with chromosomal translocations whose expressed fusion proteins have putative roles in splicing (6, 7).

Fusion proteins produced by chromosomal translocations in sarcomas often contain the amino-terminal portion of EWS and are classified as transcription factors due to the presence of a canonical carboxyl-terminal DNA-binding domain (6). EWS-FLI1 is a well-established ES oncoprotein and is recognized as a DNA-binding transcriptional regulator (8, 9). The EWS-FLI1 fusion protein of Ewing sarcoma (ES) is an example of a fusion protein whose DNA gene targets have been comprehensively investigated, yet dysregulation of these target genes induced or repressed by EWS-FLI1 does not fully explain the disease phenotype (10). In addition, some data suggest that DNA binding is not required for transformation by EWS-FLI1 (11, 12).

We recently showed that EWS-FLI1 directly binds RNA and interferes with the activity of RNA helicase A (RHA) (13). In addition, previous protein interaction studies identified the SF1 and U1C splicing factors as partners of EWS-FLI1 and discovered that EWS-FLI1 alters the splicing of an adenoviral transcript (14, 15). Also, EWS-FLI1 has been shown to modify the *IGFBP3* mRNA half-life (16) as well as directly slow the rate of RNA polymerase activity during cyclin D transcription, leading to a more oncogenic isoform, cyclin D1b (17). In total, these studies suggest functionally significant EWS-FLI1 activity in addition to transcriptional regulation driven by DNA binding (16). Thus, further resolution of EWS-FLI1 biology through protein partners is necessary to clarify its full complement of activity as an oncoprotein.

The study of complete protein networks remains challenging because it is difficult to modify single interactions while preserving overall network architecture (18). Fusion proteins are ideal as both models of oncogene function as well as targets for anticancer therapy. However, creating small-molecule inhibitors

Significance

Alternative splicing of RNA allows a limited number of coding regions in the human genome to produce proteins with diverse functionality. Alternative splicing has also been implicated as an oncogenic process. Identifying aspects of cancer cells that differentiate them from noncancer cells remains an ongoing challenge, and our research suggests that alternatively spliced mRNA and subsequent protein isoforms will provide new anticancer targets. We determined that the key oncoprotein of Ewing sarcoma (ES), EWS-FLI1, regulates alternative splicing in multiple cell line models. These experiments establish oncogenic aspects of splicing that are specific to cancer cells and thereby illuminate potentially oncogenic splicing shifts as well as provide a useful stratification mechanism for ES patients.

Author contributions: S.P.S., A.Ü., and J.A.T. designed research; S.P.S., G.T.G., and H.V.E. performed research; U.D., T.G.N., A.D., S.Y., X.L., M.T.P., M.E.L., C.H.W., and E.R.L. contributed new reagents/analytic tools; S.P.S. and G.T.G. analyzed data; and A.Ü. and J.A.T. wrote the paper.

Conflict of interest statement: United States Patent and Trademark Office awarded patent for YK-4–279 to Georgetown University; inventors include A.Ü. and J.A.T. A license agreement has been executed between Georgetown University and Tokalas, Inc. for these patents, in which J.A.T. is a founding shareholder.

This article is a PNAS Direct Submission.

[1]To whom correspondence should be addressed. Email: jat42@georgetown.edu.

This article contains supporting information online at www.pnas.org/lookup/suppl/doi:10.1073/pnas.1500536112/-/DCSupplemental.

that disrupt a specific protein–protein interaction remains a significant challenge (19, 20). We have validated a small molecule probe, YK-4–279, an enantio-specific inhibitor that both disrupts RHA interaction from EWS-FLI1 and restores RHA helicase activity (13, 21, 22). Reagents that specifically disrupt spliceosomal protein interactions are useful for the characterization of spliceosomal networks as well as understanding oncogenic aspects of posttranscriptional modifications.

Here we describe an unbiased, in-depth, proteomic analysis of EWS-FLI1 protein partners that focuses on alternative splicing. Our analysis includes protein partner identification, functional classification, experimental validation, and placement of these identified proteins into the splicing network. We report that EWS-FLI1 not only has multiple direct connections within the spliceosome but also drives aberrant splicing in cell line models that have strong correlations with ES patient tumor samples. YK-4–279 is a critical probe in these experiments as it disrupts EWS-FLI1 protein interactions, subsequently altering mRNA splicing. The mechanism and effect of aberrant splicing driven by EWS-FLI1 provide insights into the oncogenic nature of protein isoforms of CLK1, Caspase-3, Liprin-β-1, and TERT. In addition, our resolution of the EWS-FLI1 protein network that links alternative splicing with transcription provides perspective into a systems biology model involving an oncogenic fusion protein, as well as additional opportunities for targeted therapeutics.

Results

EWS-FLI1 Interacts with Proteins in Many Functional Pathways. A comprehensive analysis of protein partners of EWS-FLI1 has not been reported. Therefore, we used an unbiased approach to identify and validate potential protein interaction partners for EWS-FLI1 (*SI Appendix*, Fig. S1). Briefly, recombinant EWS-FLI1 was immobilized on an affinity column followed by the addition of ES nuclear lysate, elution, PAGE separation, and identification of bound proteins using liquid chromatography–mass spectrometry (MS). We identified 547 proteins as potential participants in EWS-FLI1 complexes (*SI Appendix*, Table S1), which were categorized using iProXpress (23) for both gene ontogeny (GO) and Kyoto Encyclopedia of Genes and Genomes (KEGG). The largest fraction of EWS-FLI1 interacting proteins were categorized as members of RNA splicing and processing families, as identified by the GO term "RNA splicing and processing" (43%, raw $P = 5 \times 10^{-55}$, Fig. 1*A*), or were members of the spliceosome complex, as identified by the KEGG category "spliceosome complex" (29%, raw $P = 2 \times 10^{-31}$, Fig. 1*B*).

The set of identified proteins were mapped using Ingenuity Pathway Analysis (IPA), which elucidated multiple networks of posttranscriptional RNA processing and spliceosome regulation (Fig. 1 *C*–*E*). Thirty-four of the 547 proteins identified as being in complex with EWS-FLI1 correspond to networks that have spliceosomal activity (Fig. 1*C*). Fifteen of the identified proteins mapped to a complex that regulates transcription factor MYC activity (Fig. 1*D*), and although MYC was not itself identified, it is highly expressed and vital in ES (24, 25). Our prior identification of RHA (*DHX9*) as an EWS-FLI1 partner was confirmed in an EWS-FLI1 interactome that shows nine proteins in a network that impacts RNA polymerase II (Fig. 1*E*). Thus, our results show that EWS-FLI1 interacts with the spliceosome, providing a previously unidentified framework for the investigation of oncogenic alternative splicing.

EWS-FLI1 Integrates into the Spliceosome Network. We focused on 13 of the proteins with known spliceosome function and validated their interactions with EWS-FLI1 to avoid MS false positives (26). Proteins that could be analyzed using commercially available antibodies were evaluated by coimmunoprecipitation (co-IP) with EWS-FLI1 using nuclear lysate from TC32 cells, a well-characterized ES cell line. An anti-FLI1 antibody was used for EWS-FLI1 co-IP, as ES cells do not express wild-type (WT) FLI1 (27). Of the spliceosomal proteins validated by co-IP, 12 of 13 identified in an EWS-FLI1 complex were confirmed (*SI Appendix*, Table S2 and Fig. S2*A*). These complexes were then reciprocally evaluated using co-IP with antibodies to PRPF8 or p68 (DDX5), in which all 13 proteins were identified in at least one of these complexes (*SI Appendix*, Table S2 and Fig. S2*A*). Eight of the 15 EWS-FLI1 complex proteins remained fully bound following RNase A treatment, whereas 3 showed decreased binding and 4 were lost from the complex (*SI Appendix*, Fig. S2*B*). In contrast, immunoprecipitation with an EWS antibody, whose epitope was in the carboxy region of the protein, identified only 10 of the 15 proteins found with EWS-FLI1, and all but DDX5 were reduced or lost with RNase A treatment (*SI Appendix*, Fig. S2*B*). These results show that EWS-FLI1 demonstrates specificity in its protein complexes with PRPF6, CDC5L, PRPF8, hnRNP K, and snRNP200 that are not found in WT EWS complexes and SFRS3 that does bind to EWS, but only in an RNA-dependent fashion (*SI Appendix*, Fig. S2*B*).

We obtained recombinant purified protein for nine of the proteins that we validated to be in complex with EWS-FLI1 in ES cells (*SI Appendix*, Table S2). In these ELISA experiments, three novel protein partners were identified as having direct interactions with EWS-FLI1: PRPF6, p68 (DDX5) and hnRNP K (*SI Appendix*, Table S2 and Fig. S3). RHA, previously identified as a direct partner of EWS-FLI1 (27) was confirmed using a RHA-specific antibody (*SI Appendix*, Table S2 and Fig. S3). In summary, a combination of co-IP and ELISA validated 13 novel proteins in complex with EWS-FLI1, including four direct interacting partners; these data confirm a highly interactive network supporting EWS-FLI1 as part of the spliceosome.

Current interaction network databases do not include fusion proteins, and thus functional analysis is challenging. Our data allowed us to draw a new protein interaction network that now includes EWS-FLI1 (Fig. 1*F*). This network connects EWS-FLI1 to its direct and indirect spliceosomal protein partners. We overlayed the spliceosomal subunit associations to indicate that EWS-FLI1 connects to U1 through p68 (DDX5), U5 through PRPF6, U2 indirectly through SF3A2, and U4/U6 indirectly through PRPF3. To our knowledge, this is the first network model that connects the spliceosome to an oncogenic fusion protein transcription factor.

Expression of EWS-FLI1 Corresponds to Alternatively Spliced Transcripts. The combined evidence from validated EWS-FLI1 interactions with multiple proteins in the spliceosome led us to investigate whether the expression of EWS-FLI1 influences alternative splicing. Three models of EWS-FLI1 were evaluated by Affymetrix GeneChip Human Exon 1.0 ST microarray: (*i*) ES TC32 cells where EWS-FLI1 was reduced with a lentiviral shRNA; (*ii*) A673i, which has a doxycycline-inducible shRNA to reduce EWS-FLI1 expression to screen for alternative splicing as measured by exon-specific expression changes; and (*iii*) human mesenchymal stem cells (hMSC), a putative cell of the origin of ES-expressing EWS-FLI1 (28) (*SI Appendix*, Fig. S4*A*). The shRNA reduction did not reduce EWS levels nor did it affect FLI1, which is not expressed in ES (*SI Appendix*, Fig. S4*A*). Two different analytical tools, Partek Genomics Suite (PGS) and easyExon, used exon expression levels to identify alternatively spliced transcripts with and without differential transcript expression (29).

Exon array analysis comparing TC32, A673i, and hMSC cell line models detected 201 common genes with alternatively spliced transcripts. We compared exon expression across 82 of these 201 (40%) common genes and show examples of six genes that have alternatively spliced transcripts in the WT control vs. shRNA-reduced EWS-FLI1 TC32 cells (Fig. 2*A*). The pattern of exon expression indicates alternative splicing when there is divergent probeset expression between the WT control expressing EWS-FLI1 (red line) and EWS-FLI1 loss (blue line). These events are indicated as a solid arrowhead with differential slopes of the line connecting two probeset expression points. To support the role of EWS-FLI1 in alternative splicing, EWS-FLI1 was expressed in hMSC, and this model shows similar patterns when EWS-FLI1 is expressed (red line) compared with the hMSC without EWS-FLI1 (blue line, Fig. 2*B*).

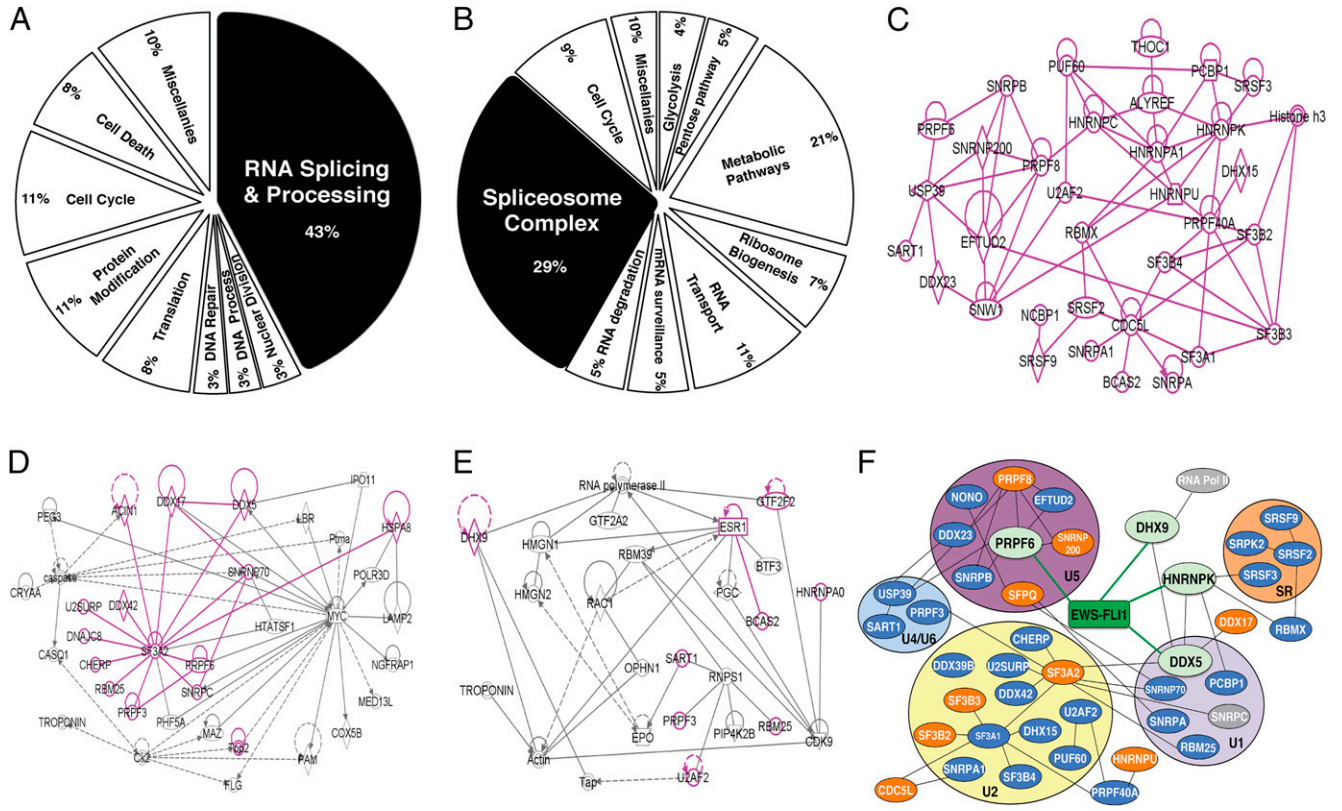

Fig. 1. EWS-FLI1–interacting proteins are highly enriched in RNA processing. (*A*) GO classification for biological processes of MS-identified proteins. (*B*) KEGG pathway analysis of MS-identified proteins. (*C*) IPA network analysis shows the interactions between spliceosome proteins identified by MS (purple). Solid purple line indicates edges connecting proteins identified by MS. Transcriptional regulators (oval), enzymes (rhombus), complex (double circle), translation regulators (hexagon), transporters (trapezoid), and cytokines (square). IPA used direct (solid line) and indirect (dotted line) data to show predicted interactions between the proteins. Arrows represent regulation. (*D*) IPA-drawn MYC network showing EWS-FLI1–interacting proteins identified by MS and their direct and indirect interactions (key as in *C*). (*E*) IPA-drawn network shows role of RNA pol II in the interactome consisting of several proteins including enzymes, nuclear receptors, and transcriptional regulators identified by MS (key as in *C*). (*F*) Proteins validated by ELISA that directly bind to EWS-FLI1 are indicated by green shading, and their direct connection by green solid lines. Immunoprecipitated-validated indirect binding partners are in orange. MS identified proteins as potential partners but not validated by co-IP are in blue. Proteins predicted to occupy nodes in EWS-FLI1 but not identified by MS are in gray. Spliceosomal complex proteins are grouped and shaded based on published associations with spliceosomal subunits.

To broaden our validation of alternative splicing, site-specific exon expression changes for the 82 common genes were evaluated by qRT-PCR. Individual loci identified by Partek analysis were validated using a reference locus (open arrowhead) compared with the region of predicted alternative splicing (closed arrowhead, Fig. 2). Expression at the reference locus of each gene was used to normalize expression to 1.0, shown on each graph by a horizontal black line (*SI Appendix*, Fig. S5). Relative expression at the region of predicted alternative splicing is shown when EWS-FLI is present (red bar) or absent (blue bar). One set of genes demonstrated alternative splicing without changes in overall gene expression levels; however, a second set showed differential overall gene expression in the presence of EWS-FLI1. Of the 82 genes evaluated, 76 (93%) confirmed consistent exon behavior with that predicted from the exon array using PGS and easyExon analysis, whereas 6 (7%) were not consistent based on the exons evaluated.

We selected 19 of the 82 genes (selected based on a literature review for having roles in oncogenesis) for confirmation across a larger panel of EWS-FLI1 cell line models (5 ES and hMSC+ EWS-FLI1). Thus, for each of these, PCR primers [based on RNA-seq de novo guided transcript reconstruction (*SI Appendix*, *Methods*)] were designed both for an exon common to all isoforms and for isoform-specific exons. We define a ES alternative splicing panel by evaluating these 19 genes in five ES cell lines with and without shRNA reduction of EWS-FLI1 (TC32, TC71, A4573, SK-ES, and STA-ET-7.2) as well as in WT and EWS-FLI1–expressing hMSC (*SI Appendix*, Fig. S4*A*). Using isoform-specific qRT-PCR primers, we determined that 10 genes (*ARID1A*, *RUNX2*, *EZH2*, *TERT*, *CUL4A*, *CAV3*, *CALD1*, *HDAC8*, *USP2*, and *IGFBP3*) fully gain or lose an isoform or demonstrate alternative promoter selection based on the modulation of EWS-FLI1 expression (Fig. 2*C*, green boxes). The variability of spliced isoforms among ES cell lines, despite all expressing EWS-FLI1, is considered in the *Discussion*. Nine of the 10 genes were consistent in hMSC expressing EWS-FLI1 as well as in three of five ES cell lines. These 10 confirmed genes represent a subset of the alternative splicing induced by EWS-FLI1, whereas 9 genes did not demonstrate changes consistent with annotated isoforms (*RUNX1*, *MBNL1*, *DACT3*, *DHX29*, *CDKN1C*, *CCND1*, *DCP2*, *BRF1*, and *DIDO1*).

Retained Introns and Skipped Exons Are Altered by EWS-FLI1. We analyzed TC32 cells with reduction of EWS-FLI1 compared with YK-4–279 treatment, a small-molecule inhibitor of EWS-FLI1, using RNA-seq as a more comprehensive analytical tool to evaluate transcriptome-wide splicing changes. Global evaluation of splicing events, including nonannotated events generated from transcriptome reconstruction, was calculated as a percentage of the top five events. The majority of splicing events in WT cells involve skipped exons (SE: 53%, Fig. 3*A*). Upon EWS-FLI1 reduction or YK-4–279 treatment, this percentage dropped to 48.5%. Retained introns (RI) almost doubled from 10% to 17.5% and 18%, respectively, for EWS-FLI1 reduction and YK-4–279

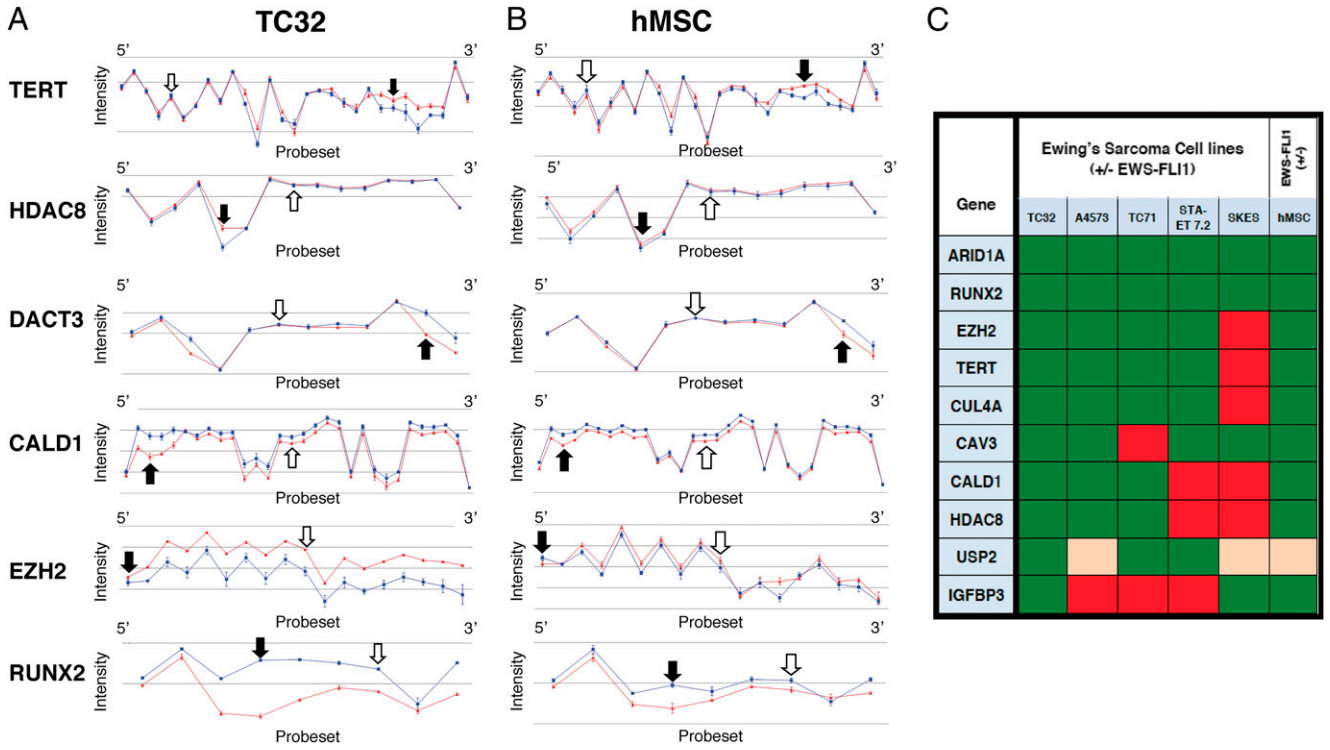

Fig. 2. Exon expression patterns and overall gene expression are altered by EWS-FLI1. (*A*) Partek genome analysis of the exon array probe set shows relative exon-level expression across genes. Each point is the expression at a single probeset (nodes). The *y* axis indicates relative intensity of exon expression, and the *x* axis indicates each probeset in 5′ to 3′ direction. TC32 WT control, express EWS-FLI1 (red) is compared with shRNA EWS-FLI1 reduction (blue). To validate alternative splicing, qRT-PCR primers were prepared based on probesets showing AS (closed arrows). Open arrows indicate a region of the transcript of equal exon expression used for primer design to normalize intensity across each gene. (*B*) Partek analysis of exon expression in hMSC with EWS-FLI1 expression (red) and absence, control WT hMSC (blue) similar to *A*. (*C*) Cellular models of ES were evaluated for a gene set using qRT-PCR with primer identification based on examples in *A*. Across the top are five ES cell lines and hMSC ± EF. The gene list is shown in the first column. Those genes with alternative splicing similar to EWS-FLI1 are shown in green, no isoform switch in red, and inconclusive qRT-PCR in light orange.

treatment. Other splicing events—mutually exclusive exons (MXE), alternative 5′ splice site (A5SS), and alternative 3′ splice site (A3SS)—did not demonstrate consistent changes between conditions nor did they have the same magnitude as the increase in retained introns (Fig. 3*A*).

The above analysis is based on the de novo transcriptome from RNA-seq; therefore, we also determined splice events corresponding only to annotated events in the Ensembl, UCSC, and RefSeq references for GRCh37, for both EWS-FLI1 reduction and YK-4–279 treatment, with common genes shaded in blue (*SI Appendix*, Table S3 *A* and *B*). The significance of overlap between the shEWS-FLI1 and YK-4–279 groups based on annotated splice events was significant for SE ($P = 3.7 \times 10^{-23}$), RI ($P = 2.5 \times 10^{-8}$), MXE ($P = 4.8 \times 10^{-5}$), A5SS ($P = 1.9 \times 10^{-5}$), and A3SS ($P = 2.6 \times 10^{-4}$).

We show three examples of alternative splicing based on reduction of EWS-FLI1 expression as well as the calculated percent spliced-in (PSI) from RNA-seq in the graph, with 95% confidence limits, and the corresponding semiquantitative RT-PCR densitometry PSI determination below each gel image (Fig. 3*B*). *CLK1* shows both a retained intron on both ends of exon 4 and a skipped exon 4 (PSI reduced from RNA-seq 85 to 52% and semiquantitative RT-PCR 86 to 69%). *CASP3* shows a skipped exon 2 (PSI reduced from RNA-seq 49 to 17% and semiquantitative RT-PCR 21 to 3%), and *PPFIBP1* shows a skipped exon 19 (PSI reduced from RNA-seq 42 to 9% and semiquantitative RT-PCR 72 to 6%) when EWS-FLI1 is expressed. Two other genes, *EZH2* and *CALD1*, were evaluated by semiquantitative RT-PCR based on primers designed for isoform-specific detection and RNA immunoprecipitation. Both demonstrated multiple isoform changes and likely alternative promoter use based on the reduction of EWS-FLI1 (*SI Appendix*, Fig. S4*C*). None of these splicing changes were observed with shRNA reduction of WT EWS protein in TC32 cells (*SI Appendix*, Fig. S4*B*).

Cross-linking immunoprecipitation (CLIP) of EWS-FLI1 was used to determine a motif associated with EWS-FLI1 binding to RNA. This motif (Fig. 3*C*) occurred more frequently within 3 nt of the 5′ exon–intron boundary than any other place ± 500 nt at either the 5′ and 3′ ends of exon–intron boundaries (Fig. 3*D*). To evaluate a second method by which EWS-FLI1 may interact with RNA, we determined the potential RNA secondary structure preference of EWS-FLI1 using local secondary structure prediction (30, 31). Using sequenced CLIP reads greater than 20 nt, we calculated the minimum free energy (MFE) structures that were possible and compared them to those generated from a random set of exonic reads of the same length (Fig. 3*E*).

We evaluated the effect on spliced isoforms of reducing EWS-FLI1 splicing partners p68 (DDX5), hnRNP K, and PRPF6 (*SI Appendix*, Fig. S4*B*). Alternative splicing for each of *CLK1*, *CASP3*, and *PPFIBP1* occurred secondary to each of the protein reductions with almost similar PSI to that of EWS-FLI1 reduction (Fig. 3*F*). Additional isoform switching occurred with reduction of p68 in 5 of 10 targets, of hnRNP K in 4 of 10, and of PRPF6 in 3 of 10 (*SI Appendix*, Fig. S4*B*). None of the spliceosomal protein reductions significantly changed the EWS-FLI1 expression levels in TC32 cells (*SI Appendix*, Fig. S4*B*). As controls for specificity, SF3A2, an indirect partner of EWS-FLI1 (Fig. 1*F*) was reduced and did not demonstrate any of the isoform switching observed after reduction of direct partners (*SI Appendix*, Fig. S4*B*). Using a further specificity control, reduction of PRPF6 in MDA-MB-231 breast cancer cells did not result in isoform switching (*SI Appendix*, Fig. S4*B*).

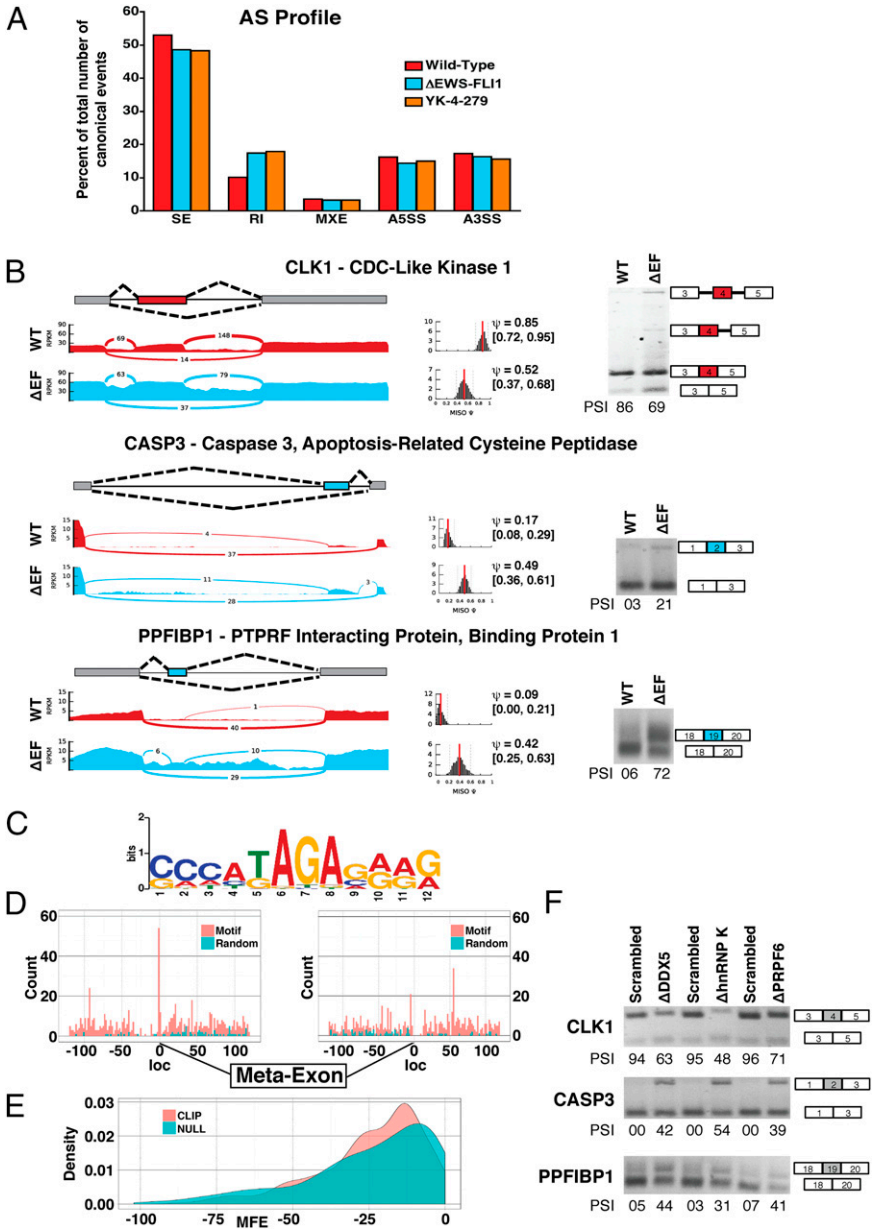

Fig. 3. Alternatively spliced genes by EWS-FLI1 impact diverse cellular processes. (*A*) Comparison of de novo transcriptome reconstruction of TC32 WT, shRNA EWS-FLI1, and YK-4–279 treatment. Classification of alternative splicing events includes skipped exons (SE), retained introns (RI), mutually exclusive exons (MXE), alternative 5′ splice sites (A5SS), and alternative 3′ splice sites (A3SS). Each type of event is quantified as a percentage of the top six events. The top six events in each sample type constitutes ∼80% of all splicing patterns found in each sample, with the remaining 20% being more complex versions of these five basic types. (*B*) Exon-centric RNA-seq coverage maps of exons affected by EWS-FLI1. The numbers of exon junction reads are indicated adjacent to the connecting bars of the coverage map. Schematic and exon-centric coverage maps showing read depth [reads per kilobase of transcript per million reads mapped (RPKM)] for *CLK1*, *CASP3*, and *PPFIBP1*. Exon annotation was derived from GRCh37 annotation. Mixture of Isoforms (MISO) was used to estimate PSI values for each annotated event. Each event has associated 95% confidence intervals. On the right, PCR validation gels associated with each splicing event were used to calculate the PSI, shown below each lane. (*C*) Multiple EM for Motif Elicitation (MEME) was used to generate a motif from CLIP reads. (*D*) Sequence regions ± 125 bp from exon–intron junctions at 5′ and 3′ ends were searched for occurrences of this motif (red). A random motif was generated for comparison of occurrence by chance (blue). The peak shows high-frequency localization of EWS-FLI1 at the 5′ intron–exon boundary. (*E*) RNA secondary structure within a 200-bp window was based on the minimum free energy (MFE) which was calculated for all CLIP reads sequenced (red). A null set was generated by randomly sampling exonic regions of the same length as the sequenced reads (blue). (*F*) PCR products of alternatively spliced exons of *CLK1*, *CASP3*, and *PPFIBP1* based on shRNA reduction of DDX5, hnRNP K, and PRPF6 in TC32 cells with their corresponding scrambled controls in alternating lanes. The PSI of exon inclusion is shown below each lane.

***TERT* Is Alternatively Spliced by EWS-FLI1, Leading to an Isoform with Enhanced Activity.** TERT, a critical regulator of telomeres leads to immortalization through both scaffolding of protein partners and enzymatic activity. Using the exon array data, we identified *TERT* as alternatively spliced, leading to the loss of exon 11 when EWS-FLI1 is reduced (Fig. 4*A*). Using primers specific to exon 11, semiquantitative RT-PCR analysis confirmed a PSI reduction from 100% to 21%, leading to the γ-TERT isoform (Fig. 4*B*). A synthetic minigene containing ∼600 bp (300 bp on either side of the exon–intron junction region) of introns 10 and 11 (Fig. 4*C*) was spliced consistently with our experimental evidence when expressed in either WT ES or EWS-FLI1 reduced cells (Fig. 4*D*). *TERT* was consistently spliced in four of five ES cell lines and hMSC that express EWS-FLI1 (Fig. 2*C*). Semiquantitative RT-PCR and minigene analysis confirmed the isoform switching because *TERT* had few mapped reads (Fig. 4*E*). RNA IP also corroborated that *TERT* mRNA binds to EWS-FLI1 (Fig. 4*F*), but not to *RUNX1* as a control (*SI Appendix*, Fig. S4*A*). We therefore evaluated telomerase activity of TERT with a telomeric repeat amplification protocol (TRAP) assay and showed that ES cells with EWS-FLI1 reduction exhibited increased TERT activity (Fig. 4*G*). Reduction of TERT protein reduced TRAP activity to 20% of control, and with re-expression of WT *TERT* the endogenously expressed protein exhibits TRAP activity at 95% of WT control. However, expression of γ-TERT led to TRAP activity that was 180% greater than that of the control, similar to the observed TRAP activity upon EWS-FLI1 reduction (Fig. 4*G*). Both WT TERT and γ-TERT were expressed from the same plasmid backbone to control for differences in expression.

YK-4–279 Disrupts EWS-FLI1 Protein Interactions Within the Spliceosome Leading to Alternative Splicing. One of our underlying hypotheses suggests that dissociation of EWS-FLI1 from specific complexes rather than reduction of expression would have differential cellular effects. EWS-FLI1 modulates a series of direct target genes, yielding a characteristic transcriptional signature that has been associated with EWS-FLI1 transformation (10). We confirmed transcript level alterations of a panel of genes using qRT-PCR analysis following shRNA reduction of EWS-FLI1 in TC32 cells. Target genes normally suppressed by EWS-FLI1 (*TGFβR2* and *IGFBP3*)

increased when EWS-FLI1 was reduced, and genes whose expression is increased by EWS-FLI1 (*VEGFA*, *NR0B1*, *CDKN1C*, *TERT*, *ID2*, *EZH2*, *UPP1*, *GLI1*, *PTPL1*) decreased in the absence of EWS-FLI1 (Fig. 5*A*). The panel of EWS-FLI1 transcriptional targets evaluated in TC32 cells treated with YK-4–279 for 8 h showed that only *VEGFA* and *TGFβR2* transcripts were altered in a fashion consistent with EWS-FLI1 reduction (Fig. 5*A*). The remainder of the transcripts in TC32 cells treated with YK-4–279 demonstrated a minimal increase in their relative expressions, independent of their changes with EWS-FLI1 protein reduction. An additional ES cell line, TC71, treated with YK-4–279, also lacked significant changes in the putative EWS-FLI1 transcriptional signature, corroborating our TC32 results (*SI Appendix*, Fig. S6).

We found that YK-4–279 prevents only the binding of direct protein partners p68 (DDX5) and RHA. Neither direct protein interactors hnRNP K and PRPF6 (Fig. 5*B*) nor indirect protein complex members PRPF8, snRNP200, SFPQ, CDC5L, and hnRNP U were blocked from EWS-FLI1 by YK-4–279 (*SI Appendix*, Fig. S7). Using the exon-array–generated EWS-FLI1 splicing panel, we found that 7 of 10 genes were similarly alternatively spliced following YK-4–279 treatment compared with EWS-FLI1 reduction (Fig. 5*C*). In addition, *CLK1*, *CASP3*, and *PPFIBP1* were all alternatively spliced with similar PSI following YK-4–279 treatment compared with EWS-FLI1 reduction (Fig. 5*D*). To control for nonspecific effects from transcription inhibition or pause, we used both doxorubicin, a known topoisomerase II inhibitor that inhibits transcription (32) and direct measurement of transcript elongation with BruDRB-seq [bromouridine labeling followed by sequencing of uridine-incorporated transcripts (33)]. None of the 13 genes evaluated showed doxorubicin-induced splice alterations with these primers, demonstrating that generalized inhibition of transcription does not recapitulate the splice changes associated with loss of EWS-FLI1 (Fig. 5 *C* and *D*). We also evaluated whether YK-4–279 would affect spliced isoforms based on altering the rate of RNA pol II elongation using BruDRB-Seq (34). ES cells in either the presence or absence of EWS-FLI1 did not change their rate of elongation when treated with YK-4–279 (Fig. 5*E*). These data demonstrate that small-molecule YK-4–279 specifically alters splicing based on altering protein interactions with patterns that are most consistent with disruption of p68 (DDX5) or RHA from EWS-FLI1.

Tumors from ES Patients Demonstrate Similar EWS-FLI1–Influenced Splicing. Alternative splicing in human tumors is becoming recognized as a driver of myelodysplasia (35, 36). We therefore analyzed exon array data obtained from 75 ES patient tumor samples (ESTS) before chemotherapy to determine if these clinical samples would match mRNA expression profiles generated by ES cell line models. Individual probeset expression from ESTS was normalized by overall gene expression and then compared between neural crest (NC), hMSC, and TC32 with/without EWS-FLI1. Both NC and hMSC have been putatively evaluated as the ES cell of origin (28, 37, 38). Using the paired cell line models, we were able to calculate ANOVA P values for each probeset to measure the significance of a consistent effect of EWS-FLI1 across models. There were 21 events based on EWS-FLI1 expression across the cell line models that were significantly altered ($P \leq 0.05$ after Benjamini–Hochberg correction). The expression of EWS-FLI1 in both NC and hMSC caused alternative splicing changes similar to EWS-FLI1 in TC32 and ESTS (Fig. 6*A*). There were 5,595 events when comparing TC32 with EWS-FLI1 reduction to ESTS ($P \leq 0.05$ after Benjamini–Hochberg correction). The overlap between the cell line models and ESTS analysis is highly significant ($P = 0.000717$). We show a panel of genes that demonstrates the similarities of exon expression (*SI Appendix*, Fig. S8*A*). As a control, exon expression patterns for 10 of the ES alternatively spliced transcripts were evaluated in the breast cancer cell line MDA-MB-231. Eight of the 10 genes show alternative transcripts, based on the regions in the gray boxes, at sites where alternative splicing patterns differ from those found in ES (*SI Appendix*, Fig. S8*B*).

Principal component analysis (PCA) for all alternatively expressed exons suggesting splice variants was normalized for overall gene expression across all genes among 53 of the 82 patients from whom we obtained clinical presentation and relapse data. ES patients with both localized and metastatic disease without recurrence events tend to segregate based on specific exon expression patterns from patients with recurrence when global splicing profiles are considered. Gene-normalized exon expression patterns allow separation of localized patients who experience a recurrence from those who do not recur (Fig. 6 *B* and *D*). Chi-squared testing of clusters generated by hierarchical clustering of gene-normalized exon expression showed near-significant differences for patients with localized (Fig. 6 *B* and *C*; $P = 0.1$) and metastatic (Fig. 6 *D* and *E*; $P = 0.05$) disease between groups of patients who experienced an event and those who did not. Thus, analysis of these ESTS suggests that alternative splicing patterns may be associated with patient outcome despite their universal expression of EWS-FLI1.

Discussion

The canonical model of EWS-FLI1 transformation suggests that the DNA-binding domain is bound to promoter sequences as a transcriptional regulator (9, 28, 39, 40); however, full phenotypic recapitulation of ES through the manipulation of differentially expressed genes alone has not been accomplished. Our data show an emergent network of EWS-FLI1, derived from analysis of protein–protein interactions, including discovery of p68 (DDX5), PRPF6, and hnRNP K as direct binding partners. We validated EWS-FLI1–modulated splicing across a panel of ES models, as well as hMSC cells expressing EWS-FLI1, and found consistent splice variants in the presence of EWS-FLI1. The small molecule

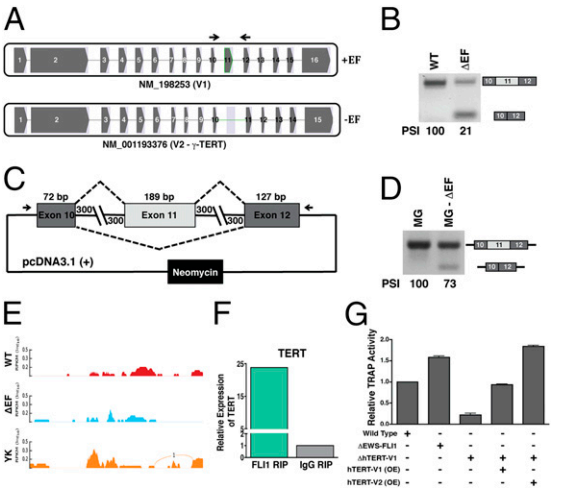

Fig. 4. TERT is alternatively spliced to generate an isoform with enhanced telomerase activity. (*A*) Isoform-specific *TERT* semiquantitative RT-PCR primer locations are indicated by the forward and reverse arrows based on exon array analysis. The exons are indicated by gray boxes and exon-specific splice changes of skipped exon by the green line. (*B*) TC32 ± EWS-FLI1 mRNA semiquantitative RT-PCR products using primers shown in *A*. The PSI of exon 11 inclusion are shown below each lane. (*C*) Schematic of the TERT minigene (MG), indicating exons 10, 11, and 12 including 300 bp on the either side of the exon–intron junction regions of introns 10 and 11. Minigene-specific PCR primer locations are indicated by forward and reverse arrows. (*D*) Minigene (MG) plasmids were transfected into TC32 WT or shRNA EWS-FLI1–reduced cells. PCR products using MG-specific primers are shown. (*E*) Exon-centric coverage map for TERT was generated from deep sequencing described (Fig. 3*B*). (*F*) RNA immunoprecipitation (RIP) showing the presence of TERT mRNA bound to EWS-FLI1 compared with total 18S vs. IgG control IP. (*G*) Telomerase activities were analyzed by TRAP assay. TC32 WT, shRNA EWS-FLI1, shRNA hTERT with or without re-expression of WT TERT, or expression of γ-TERT were analyzed in real-time TRAP assays.

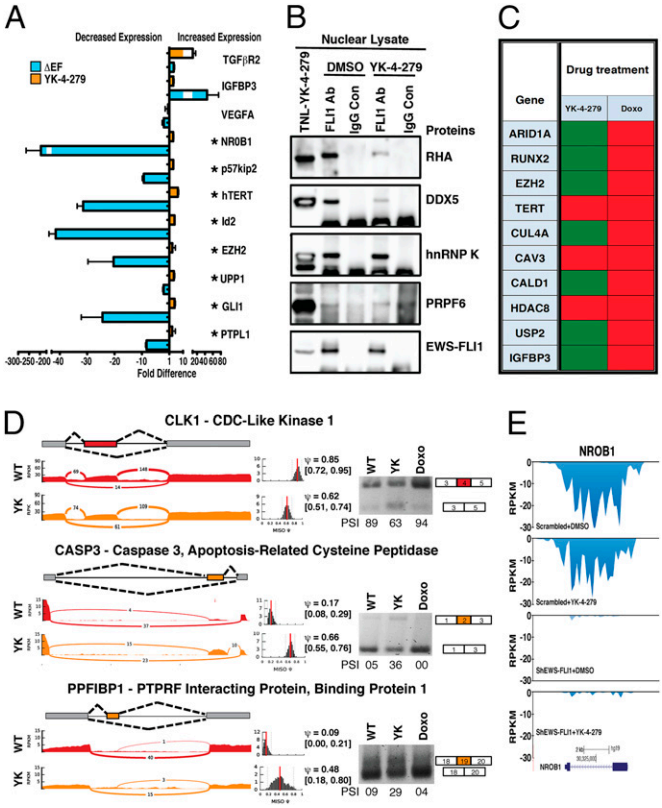

Fig. 5. YK-4–279 treatment of ES cells reverts EWS-FLI1–modulated alternative splicing changes and does not mimic transcriptional effects of EWS-FLI1 reduction. (*A*) A qRT-PCR gene expression panel for canonical EWS-FLI1 transcriptional targets compared WT TC32, EWS-FLI1 reduction (ΔEF, blue bars), and YK-4–279 treatment (orange bars). Graph shows relative fold expression calculated using ΔΔct value changes from WT (set at 1.0). **P* = 0.04 (NR0B1), 0.001 (p57), 0.003 (hTERT), 0.03 (Id2), 0.03 (EZH2), 0.006 (UPP1), 0.02 (GLI1), and 0.003 (PTPL1). (*B*) EWS-FLI1 was immunoprecipitated following treatment with YK-4–279 or DMSO control in TC32 cells for 15 h. The total nuclear lysate (TNL) treated with YK-4–279 was used as input control (lane 1), FLI1 antibody (lanes 2 and 4), and rabbit polyclonal IgG antibody (lanes 3 and 5). Antibodies for specific protein detection are shown to the right of each panel. (*C*) Alternative splicing screen comparing YK-4–279 and doxorubicin treatment using the same exon array identified RT-PCR primers as in Fig. 2*C*. Genes with EWS-FLI1 exon-specific isoform switch, similar to EWS-FLI1, are green, and no isoform switch is red. (*D*) Schematic and exon-centric coverage maps (RPKM) for *CLK1*, *CASP3*, and *PPFIBP1* derived from deep sequencing (key as in Fig. 3*B*). MISO was used to estimate PSI values for each annotated event, and 95% confidence intervals are shown. WT TC32 data are red, and YK-4–279 treatment is orange. To the right, PCR validation gels show the splicing change, and the PSI is calculated from densitometry and shown beneath each graph. (*E*) Elongation rates for 10 min for the NR0B1 gene following 5,6 dichloro-1-β-D-ribofuranosylbenzimidazole (DRB) removal are shown for WT TC32 cells (scrambled, *Upper* two panels) and for EWS-FLI1–reduced TC32 cells (shEWS-FLI1, *Lower* two panels). Polymerization rate was calculated following bromouridine (BRU) incorporation from the time of DRB washout. The second and fourth panels care concomitantly treated with YK-4–279 during the elongation period. Read depth (RPKM) calculated on *y* axis is based on immunoseparation of BRU-labeled message followed by deep sequencing. NROB1 transcript was derived from GRCh37 annotation shown at the bottom.

YK-4–279, originally discovered for its ability to disrupt RHA–EWS-FLI1 interaction, also disrupts p68; however, neither PRPF6 nor hnRNP K are disrupted from the EWS-FLI1 complex. The mechanism of EWS-FLI1–modulated splicing is revealed, in part, through an RNA-binding motif at intron–exon boundaries or via a binding preference for mRNA with secondary structure. The protein partners p68, PRPF6, and hnRNP K are likely coregulatory transmodulators of EWS-FLI1 on RNA splice site selection. Finally, we show that ES tumors from patients demonstrate similar exon-specific expression patterns as EWS-FLI1 cell line models, including NC and hMSC. These novel protein interactions place EWS-FLI1 in a central role as a component of the spliceosome and provide evidence to support a historical hypothesis about EWS-FLI1 influencing alternative splicing (14, 41–43). These data allow for discussion of (*i*) how EWS-FLI1 links transcription and splicing through protein networks, (*ii*) a novel mechanism for YK-4–279 inhibition of EWS-FLI1, (*iii*) how the EWS-FLI1 network differs from the WT EWS network, (*iv*) splicing as an oncogenic process, and (*v*) how differentially spliced isoforms might contribute to oncogenesis and pathogenesis.

EWS-FLI1 Links Transcription and Splicing. This study reveals multiple new protein partners of EWS-FLI1 that suggest multiple functions for this oncogene beyond direct transcriptional regulation; evidence presented here supports a role in posttranscriptional splicing regulation. EWS-FLI1 modulation of splicing could occur through direct binding to nascent mRNA to block *trans*-elements, altering the protein interaction network, or by interfering with helicase activity to alter *cis*-acting elements. Our CLIP-seq experiment confirms our recent finding that EWS-FLI1 binds to RNA, although a motif that corresponds to a canonical donor, acceptor, or branch point site was not identified. Rather, the sequence motif(s) were found at intron–exon boundaries of those genes alternatively spliced, potentially using those *cis*-elements to localize alternative protein complexes.

EWS-FLI1 binds to p68, and reduction of p68 mimics most of the EWS-FLI1 splicing events that we measured. A potentially similar mechanism occurs where mutant U1C in yeast alters the activity of the Prp28p helicase to modulate splicing (14, 44, 45). Because EWS-FLI1 interacts with multiple other spliceosomal proteins, those network proteins may also recognize different splicing elements. Consistent with this, reduction of either hnRNP K or PRPF6, direct EWS-FLI1 partners, leads to alternative splicing. PRPF6 has been independently implicated as a driver of colorectal cancer (46). However, reduction of SF3A2, which is an RNA-dependent, indirect EWS-FLI1 partner, did not alter splicing for those genes analyzed. PRPF6 reduction in breast cancer cells also did not alter splicing of EWS-FLI1 modulated genes. A final mechanism of EWS-FLI1–modulated splicing may come from direct inhibition of a partner helicase activity, which we recently demonstrated for RHA (13).

YK-4–279 Alters Splicing Rather than Direct Transcriptional Inhibition. We directly confirm a panel of EWS-FLI1 transcriptional targets that are modulated by the reduction of EWS-FLI1 levels. The discovery and optimization of YK-4–279 was initially based on its ability to block RHA from binding to EWS-FLI1. We therefore expected the effect of the EWS-FLI1 inhibitor YK-4–279 to mimic the transcriptional effects of EWS-FLI1 reduction; however, this was not observed. Instead, YK-4–279 treatment showed a significant overlap of alternative splicing events that were similar to EWS-FLI1 reduction. In addition, YK-4–279 blocks the binding of p68 as well as RHA, but does not interfere with the binding of PRPF6 or hnRNP K. Both helicases could potentially modulate splicing; however, p68 has been directly implicated in 5′ splice site selection as a function in the U1 complex (47). However, earlier work also places RHA in the spliceosome and as a regulator of splicing (48–50). This suggests that YK-4–279 blocking of specific protein interactions from EWS-FLI1, such as RHA and p68, will alter the splicing program differently from the loss of EWS-FLI1. We also considered whether EWS-FLI1–modulated RNA pol II elongation activity was affected by YK-4–279 treatment, because this mechanism led to alternative poly(A) site selection for cyclin D1 (17). We did not note any alteration in polymerase elongation activity when stalled complexes were released; however, polymerase effects based on YK-4–279 treatment cannot be fully eliminated based on this limited investigation.

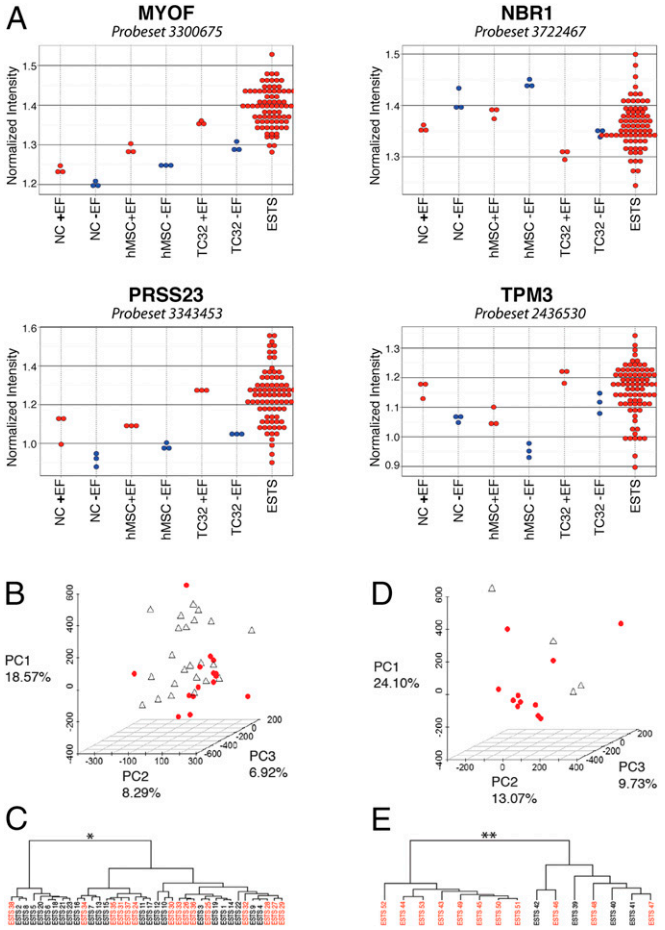

Fig. 6. Alternative splicing patterns in ESTS and TC32 have similar exon-specific expression. (*A*) Gene-normalized probeset intensity plots for NC and hMSC WT (−EF) with expression of EF (+EF) as well as TC32 cells as WT (+EF) and shRNA reduction of EWS-FLI1 (−EF), and ESTS. Each probeset has been normalized by gene expression to provide a relative measure of exon inclusion. (*B*) PCA plots based on the differential exon expression leading to alternative splicing profiles for patients with localized ES. Patients who did not experience recurrence (open triangle, black) and patients who experienced recurrence (closed circle, red) are plotted in the first three principal component dimensions. Variance in each principal component is listed along the axes. (*C*) Dendrogram clustering of first three principal components evaluating patients with localized disease illustrating weak grouping effect separating patients with (red) and without (black) recurrence (P = 0.1). (*D*) PCA plots based on the differential exon expression leading to alternative splicing profiles for patients with metastatic ES. Patients who did not experience recurrence (open triangle, black) and patients who experienced recurrence (closed circle, red) are plotted in the first three principal component dimensions. Variance in each principal component is listed along the axes. (*E*) Dendrogram clustering of the first three principal components evaluating patients with metastatic disease illustrating strong grouping effect separating patients with (red) and without (black) recurrence (P = 0.05).

We did observe changes in splicing when YK-4–279 disrupted p68 and RHA, but it did not disrupt PRPF6 or hnRNP K. However, when PRPF6 or hnRNP K expression was reduced, the alternative splicing changes showed similarity with YK-4–279 for a subset of genes (*SI Appendix*, Fig. S4*B*, compared with Fig. 5*C*). This supports our findings that these splice site modulators are part of EWS-FLI1–directed modulation of splicing, yet have different effects than that of p68 or RHA. Although larger data sets would be informative, these data suggest that a small molecule, such as YK-4–279, can be used to dissect properties of protein interactions that would otherwise remain obscured when RNAi approaches are used for functional analysis, as elimination of a protein can lead to confounding downstream effects. Treatment with doxorubicin to control for general transcriptional inhibition demonstrates that splicing alterations induced by YK-4–279 are not a secondary effect of cells dying. Thus, small-molecule inhibitors of specific protein–protein interactions will become increasingly useful in understanding the functionality and potentially oncogenic properties of the spliceosome.

Spliceosomal Network of EWS Differs from EWS-FLI1. These experiments highlight the importance of building protein interaction networks that include fusion oncoproteins. There appear to be critical differences between the canonical EWS network and our experimentally validated EWS-FLI1 network, both in their qualitative protein interactions and the dependence of RNA bridging for these complexes to form (*SI Appendix*, Fig. S2*B*). Our experiments show that reduction of EWS did not create the same splice variants as EWS-FLI1 reduction among the nine variants tested (*SI Appendix*, Fig. S4*B*). WT EWS interacts with many proteins and has a role in many cellular processes as an RNA-binding protein (51). Full-length EWS is recognized as a regulator of alternative splicing in regions of DNA damage, which involves a network of proteins different from EWS-FLI1 (52). The EWS network interactions are substantially different from EWS-FLI1 and can be visualized in silico using STRING 9.1 (53) that includes YB-1 (*SI Appendix*, Fig. S9). YB-1 was identified as a splicing protein partner of EWS that did not complex with EWS-FLI1, which was consistent with our data (41, 54). EWS also interacts with RHA (*DHX9*); however, PRPF6 and hnRNP K do not complex with EWS (*SI Appendix*, Fig. S9). PRPF6 and hnRNP K, however, do connect to RHA and YB-1 without interceding network nodes. Our data show that EWS-FLI1 directly interacts, independent of RNA, with PRPF6 and hnRNP K as well as RHA. EWS, previously reported to alter splicing (6), also alters *FAS* alternative splicing (AS); although EWS-FLI1 also leads to the same splice alteration, the PSI appears much lower (55). This supports data reporting that different complexes of proteins differentially recognize splice enhancers or suppressors; this paper provides tools to further probe this theory using alternative splicing as a model. The extent to which EWS-FLI1 perturbs the EWS network could be elucidated in future work by (*i*) further dissection of YB-1 or other protein interactions or (*ii*) evaluation of EWS inhibition on oncogenesis.

Spliceosome as Oncogenic Modulator. Before the data presented in this paper, *TERT*, *CLK1*, *CASP3*, and *PPFIBP1* were not recognized as isoforms modulated by EWS-FLI1. One prior report identified EWS-FLI1 increasing TERT activity independently of DNA binding; however, no isoform analysis was performed (56). These four genes were recognized as putative contributors to oncogenesis based on the published literature (57–65). None of these genes were alternatively spliced by WT EWS reduction.

TERT functions through a combination of direct enzymatic activity and as a protein scaffold to affect transcription as well as telomere maintenance (66, 67). We identified an EWS-FLI1–modulated splice variant of *TERT* using exon array analysis, despite very low levels of *TERT* transcription in our RNA-seq data. Native *TERT* splicing analysis in ES, *TERT* minigene splicing, and RNA IP data support a direct involvement of EWS-FLI1 in this alternative splicing. The canonical isoform of TERT includes 62 amino acids translated from exon 11 and is the predominant splice variant identified in WT ES cells expressing EWS-FLI1. However, in the EWS-FLI1–reduced cells, exon 11 is skipped and the large isoform is significantly reduced. This TERT variant has been classified as the γ-isoform, where the distal reverse transcriptase domain is shortened (68). The only functional data for γ-TERT show that cell lines Huh7 and HLE expressing very small quantities of γ-TERT have 50% greater telomerase activity than cells lacking γ-TERT (68). When EWS-FLI1 was reduced in ES cells, expression of the γ-*TERT* isoform was increased and telomerase activity also increased above baseline. To determine if this increase was due to the γ-TERT isoform, WT TERT was reduced with shRNA followed by expression of both WT and γ-TERT.

Although exogenous expression of WT TERT replaced telomerase activity to baseline, exogenous expression of γ-TERT increased activity by ∼50% over baseline. We conclude from this that EWS-FLI1 influences splicing with potential biologic consequences, and future work will be dedicated to resolving the contribution of these alternative isoforms.

Three other genes—*CLK1*, *CASP3*, and *PPFIBP1*—were consistently alternatively spliced by EWS-FLI1 and also demonstrated similar alternative splicing following reduction of EWS-FLI1 direct splicing partners. *CLK1* demonstrated both intron retention and exon skipping. The skipped exon 4 and intron retention variants are either both inactive or rapidly cleared by nonsense-mediated decay (63, 69). The loss of CLK1 activity may disrupt a feedback loop because its kinase activity is critical for the phosphorylation of multiple SR proteins that regulate splicing (63, 70, 71). The inclusion of *CASP3* exon 2 with EWS-FLI1 reduction places an internal ribosome entry site into the 5′-UTR of the mRNA (72). This 5′-UTR may enhance the translation of caspase-3, thus increasing its protein levels and in part explaining the increased apoptosis seen with YK-4–279 treatment (21). *CASP3* exon 2 has also been recognized as containing a polymorphism that increases the likelihood of head and neck cancer (61). *PPFIBP1* is a scaffolding protein where the reduction of EWS-FLI1 leads to the inclusion of exon 19, which is translated to a region between the first and second sterile alpha motif (SAM) protein interaction domain, which is critical for CASK binding (73). *PPFIBP1* has been implicated in both brain and pancreatic cancer; however, the relationship between oncogenesis and specific isoforms is not well characterized (60, 64).

Alternative Splicing in Patient Tumors Validates Modeling, May Inform on ES Oncogenesis, and Has Potential for Patient Stratification. One of the significant challenges for physicians treating patients with ES is therapeutic stratification at the time of diagnosis, beyond metastatic disease (74, 75). With many new therapeutic options in development, knowledge of those patients who will experience a tumor recurrence would allow for augmented or personalized therapy at the time of diagnosis, rather than after relapse. We were able to show, using PCA analysis of all splicing events, that there was a separation between patients with either localized or metastatic disease who do not experience a relapse and those likely to relapse. All these patients expressed EWS-ets fusions, and prior prospective investigations did not demonstrate survival differences based on the EWS-ets fusion type (76, 77). Therefore, heterogeneity in survival, based on EWS-FLI1–regulated splicing, seems counterintuitive. Our evaluation of ES cell lines, which all expressed EWS-ets (two type 1, two type 2, and one type 3), also showed some variability in spliced isoforms. This suggests that EWS-ets splicing factor partner proteins, which participate in splice site selection, could lead to alternative isoform expression that is reflected in our patient samples.

These alternative protein isoforms, generated based on tumor differences in splicing-factor levels beyond EWS-FLI1, could be responsible for differences in ES outcome. Thus, we hypothesize that patients who have recurrent disease, although all express EWS-ets, may ultimately have different oncogenesis-related protein isoforms in their tumors. The clinical data analyzed here lead to a testable hypothesis that could solve a vexing clinical challenge; this requires prospective validation with an approach sensitive to spliced isoforms, such as RNA-seq or single-molecule real-time sequencing. These deep-sequencing technologies were neither cost effective nor widely available 10 y ago when the samples analyzed for this paper were collected.

A number of studies laid important groundwork by probing the potential role of EWS-FLI1 in alternative splicing (14, 16, 41, 44). The data in this paper indicate that EWS-FLI1 impacts ES biology beyond transcriptional modulation and has a significant role in posttranscriptional regulation. This additional functionality of EWS-FLI1 is critical to consider when designing small-molecule inhibitors or other perturbants. The tools that we used to create EWS-FLI1 networks are likely exportable to other fusion protein transcription factors (7). Reducing protein levels of critical splicing partners in the EWS-FLI1 complexes and observing changes in expressed gene isoforms could be informative toward a comprehensive map of functional splicing effects. In addition, we show the effectiveness of small-molecule perturbation of protein complexes in dissecting splicing patterns. This relatively specific targeting in a model where a single protein, EWS-FLI1, connects transcription and splicing could uncover valuable components of the elusive splicing code. This work adds a level of complexity to our understanding of the role of chimeric transcription factors and provides for the possibility of novel therapeutic targets that would be both specific and highly effective.

Materials and Methods

Additional materials and methods text can be found in *SI Appendix*.

Cell Lines and Reagents. ES cell lines TC32, TC71, A4573, SKES, STA-ET-7.2, and A673i (Olivier Delattre, Institute Curie, Paris) were grown in 10% (vol/vol) FBS in RPMI at 37 °C in 5% CO_2 and passaged every 3–4 d. hMSC were obtained from Lonza. Eukaryotic EWS-FLI1 was expressed using pCIneo.EWS-FLI1. EWS-FLI1 shRNA was a generous gift from Christopher T. Denny (University of California, Los Angeles). Lentiviral stocks were made by transiently transfecting 2.7 μg of expression vector, 675 ng of VSV-G–expressing plasmid pCMV, and 2.0 μg of packaging plasmid pCMVHR8.2 deltaR. Viral stocks were collected 2 d after transfection, filtered, and frozen.

Ewing Sarcoma Tumor Samples. Patient's samples and informed consent were obtained from 43 German patients treated within the Euro-E.W.I.N.G.-99 (EE99) trial and from 14 German patients treated within the European Intergroup Cooperative Ewing Sarcoma Studies (EICESS)-92 trial (74, 78). An additional 29 samples were from patients who participated in the referenced clinical trials and signed informed consent for inclusion of their tumor in biology investigations (79). All data and informatics for this publication were obtained with coded ESTS that had all identifying information removed.

ACKNOWLEDGMENTS. We thank Anton Wellstein for careful reading and comments; Stephen Lessnick and Christopher T. Denny for plasmids; Olivier Delattre for cell line A673i; and Ryan Commins, Sarah Jaffe, Kamal Sajwan, and Lauren Scher for technical assistance. Technical support was provided by the Genome Core, Children's Hospital Los Angeles. Financial support for this research was provided by the Children's Cancer Foundation (Baltimore); St. Baldrick's Foundation; Go4theGoal Foundation; Burroughs Wellcome Clinical Scientist Award in Translational Research (to J.A.T.); and NIH Grants RC4CA156509 (to J.A.T.), R01CA133662 (to J.A.T.), R01CA138212 (to J.A.T.), R01CA134604 (to E.R.L.), and R21CA180524 (to X.L.). Support was also provided by Biostatistics and Bioinformatics, Genetics and Epigenetics, Proteomics and Metabolomics, Tissue Culture, Shared Resources, Mid-Atlantic Shared Resources Consortium by Lombardi Comprehensive Cancer Center Cancer Center Support Grant P30 CA051008-16 (Lou Weiner, PI); DKH-108128 and by Federal Ministry of Education and Research Germany (to U.D.); Bundesministerium für Bildung und Forschung (TranSaRNet), Deutsches Zentrum für Luft- und Raumfahrt e.V. 01GM0869, European Ewing Consortium (602856-2), PanCareLife (602030-2); PROVABES ERA-Net-TRANSCAN (01KT1310); and National Cancer Institute (NCI) Grant 1U01CA114757, Children's Oncology Group (NCI CA98543, CA98413).

1. Barbosa-Morais NL, et al. (2012) The evolutionary landscape of alternative splicing in vertebrate species. *Science* 338(6114):1587–1593.
2. Merkin J, Russell C, Chen P, Burge CB (2012) Evolutionary dynamics of gene and isoform regulation in mammalian tissues. *Science* 338(6114):1593–1599.
3. Kornblihtt AR, et al. (2013) Alternative splicing: A pivotal step between eukaryotic transcription and translation. *Nat Rev Mol Cell Biol* 14(3):153–165.
4. Garraway LA, Lander ES (2013) Lessons from the cancer genome. *Cell* 153(1):17–37.
5. Ellis JD, et al. (2012) Tissue-specific alternative splicing remodels protein-protein interaction networks. *Mol Cell* 46(6):884–892.
6. Kovar H (2011) Dr. Jekyll and Mr. Hyde: The Two Faces of the FUS/EWS/TAF15 Protein Family. *Sarcoma* 2011:837474.
7. Mitelman F, Johansson B, Mertens F (2007) The impact of translocations and gene fusions on cancer causation. *Nat Rev Cancer* 7(4):233–245.
8. Braun BS, Frieden R, Lessnick SL, May WA, Denny CT (1995) Identification of target genes for the Ewing's sarcoma EWS/FLI fusion protein by representational difference analysis. *Mol Cell Biol* 15(8):4623–4630.
9. Smith R, et al. (2006) Expression profiling of EWS/FLI identifies NKX2.2 as a critical target gene in Ewing's sarcoma. *Cancer Cell* 9(5):405–416.

10. Erkizan HV, Uversky VN, Toretsky JA (2010) Oncogenic partnerships: EWS-FLI1 protein interactions initiate key pathways of Ewing's sarcoma. *Clin Cancer Res* 16(16):4077–4083.
11. Jaishankar S, Zhang J, Roussel MF, Baker SJ (1999) Transforming activity of EWS/FLI is not strictly dependent upon DNA-binding activity. *Oncogene* 18(40):5592–5597.
12. Welford SM, Hebert SP, Deneen B, Arvand A, Denny CT (2001) DNA binding domain-independent pathways are involved in EWS/FLI1-mediated oncogenesis. *J Biol Chem* 276(45):41977–41984.
13. Erkizan HV, et al. (2015) RNA helicase A activity is inhibited by oncogenic transcription factor EWS-FLI1. *Nucleic Acids Res* 43(2):1069–1080.
14. Knoop LL, Baker SJ (2001) EWS/FLI alters 5′-splice site selection. *J Biol Chem* 276(25): 22317–22322.
15. Yang L, Chansky HA, Hickstein DD (2000) EWS.Fli-1 fusion protein interacts with hyperphosphorylated RNA polymerase II and interferes with serine-arginine protein-mediated RNA splicing. *J Biol Chem* 275(48):37612–37618.
16. France KA, Anderson JL, Park A, Denny CT (2011) Oncogenic fusion protein EWS/FLI1 down-regulates gene expression by both transcriptional and posttranscriptional mechanisms. *J Biol Chem* 286(26):22750–22757.
17. Sanchez G, et al. (2008) Alteration of cyclin D1 transcript elongation by a mutated transcription factor up-regulates the oncogenic D1b splice isoform in cancer. *Proc Natl Acad Sci USA* 105(16):6004–6009.
18. Csermely P, Korcsmáros T, Kiss HJ, London G, Nussinov R (2013) Structure and dynamics of molecular networks: A novel paradigm of drug discovery: A comprehensive review. *Pharmacol Ther* 138(3):333–408.
19. Koehler AN (2010) A complex task? Direct modulation of transcription factors with small molecules. *Curr Opin Chem Biol* 14(3):331–340.
20. Uren A, Toretsky JA (2005) Ewing's sarcoma oncoprotein EWS-FLI1: The perfect target without a therapeutic agent. *Future Oncol* 1(4):521–528.
21. Erkizan HV, et al. (2009) A small molecule blocking oncogenic protein EWS-FLI1 interaction with RNA helicase A inhibits growth of Ewing's sarcoma. *Nat Med* 15(7):750–756.
22. Barber-Rotenberg JS, et al. (2012) Single enantiomer of YK-4-279 demonstrates specificity in targeting the oncogene EWS-FLI1. *Oncotarget* 3(2):172–182.
23. Mittag T, Kay LE, Forman-Kay JD (2010) Protein dynamics and conformational disorder in molecular recognition. *J Mol Recognit* 23(2):105–116.
24. Bailly RA, et al. (1994) DNA-binding and transcriptional activation properties of the EWS-FLI-1 fusion protein resulting from the t(11;22) translocation in Ewing sarcoma. *Mol Cell Biol* 14(5):3230–3241.
25. Rosolen A, Toretsky J, Neckers L (1994) Antisense inhibition of CHP100 C-myc expression results in reduced in vitro growth kinetics and loss of in vivo tumorigenesis. *Prog Clin Biol Res* 385:95–101.
26. Mellacheruvu D, et al. (2013) The CRAPome: A contaminant repository for affinity purification-mass spectrometry data. *Nat Methods* 10(8):730–736.
27. Toretsky JA, et al. (2006) Oncoprotein EWS-FLI1 activity is enhanced by RNA helicase A. *Cancer Res* 66(11):5574–5581.
28. Tirode F, et al. (2007) Mesenchymal stem cell features of Ewing tumors. *Cancer Cell* 11(5):421–429.
29. Chang TY, et al. (2008) easyExon: A Java-based GUI tool for processing and visualization of Affymetrix exon array data. *BMC Bioinformatics* 9:432.
30. Hofacker IL, Priwitzer B, Stadler PF (2004) Prediction of locally stable RNA secondary structures for genome-wide surveys. *Bioinformatics* 20(2):186–190.
31. Mathews DH, et al. (2004) Incorporating chemical modification constraints into a dynamic programming algorithm for prediction of RNA secondary structure. *Proc Natl Acad Sci USA* 101(19):7287–7292.
32. Collins I, Weber A, Levens D (2001) Transcriptional consequences of topoisomerase inhibition. *Mol Cell Biol* 21(24):8437–8451.
33. Paulsen MT, et al. (2014) Use of Bru-Seq and BruChase-Seq for genome-wide assessment of the synthesis and stability of RNA. *Methods* 67(1):45–54.
34. Veloso A, et al. (2014) Rate of elongation by RNA polymerase II is associated with specific gene features and epigenetic modifications. *Genome Res* 24(6):896–905.
35. Yoshida K, et al. (2011) Frequent pathway mutations of splicing machinery in myelodysplasia. *Nature* 478(7367):64–69.
36. Papaemmanuil E, et al.; Chronic Myeloid Disorders Working Group of the International Cancer Genome Consortium (2011) Somatic SF3B1 mutation in myelodysplasia with ring sideroblasts. *N Engl J Med* 365(15):1384–1395.
37. von Levetzow C, et al. (2011) Modeling initiation of Ewing sarcoma in human neural crest cells. *PLoS ONE* 6(4):e19305.
38. Riggi N, et al. (2008) EWS-FLI-1 expression triggers a Ewing's sarcoma initiation program in primary human mesenchymal stem cells. *Cancer Res* 68(7):2176–2185.
39. Lessnick SL, Dacwag CS, Golub TR (2002) The Ewing's sarcoma oncoprotein EWS/FLI induces a p53-dependent growth arrest in primary human fibroblasts. *Cancer Cell* 1(4):393–401.
40. Prieur A, Tirode F, Cohen P, Delattre O (2004) EWS/FLI-1 silencing and gene profiling of Ewing cells reveal downstream oncogenic pathways and a crucial role for repression of insulin-like growth factor binding protein 3. *Mol Cell Biol* 24(16):7275–7283.
41. Chansky HA, Hu M, Hickstein DD, Yang L (2001) Oncogenic TLS/ERG and EWS/Fli-1 fusion proteins inhibit RNA splicing mediated by YB-1 protein. *Cancer Res* 61(9): 3586–3590.
42. Petermann R, et al. (1998) Oncogenic EWS-Fli1 interacts with hsRPB7, a subunit of human RNA polymerase II. *Oncogene* 17(5):603–610.
43. Kovar H, et al. (2001) The EWS protein is dispensable for Ewing tumor growth. *Cancer Res* 61(16):5992–5997.
44. Knoop LL, Baker SJ (2000) The splicing factor U1C represses EWS/FLI-mediated transactivation. *J Biol Chem* 275(32):24865–24871.
45. Du H, Tardiff DF, Moore MJ, Rosbash M (2004) Effects of the U1C L13 mutation and temperature regulation of yeast commitment complex formation. *Proc Natl Acad Sci USA* 101(41):14841–14846.
46. Adler AS, et al. (2014) An integrative analysis of colon cancer identifies an essential function for PRPF6 in tumor growth. *Genes Dev* 28(10):1068–1084.
47. Liu ZR (2002) p68 RNA helicase is an essential human splicing factor that acts at the U1 snRNA-5′ splice site duplex. *Mol Cell Biol* 22(15):5443–5450.
48. Li J, et al. (1999) A role for RNA helicase A in post-transcriptional regulation of HIV type 1. *Proc Natl Acad Sci USA* 96(2):709–714.
49. Fujii R, et al. (2001) A role of RNA helicase A in cis-acting transactivation response element-mediated transcriptional regulation of human immunodeficiency virus type 1. *J Biol Chem* 276(8):5445–5451.
50. Hartmuth K, et al. (2002) Protein composition of human prespliceosomes isolated by a tobramycin affinity-selection method. *Proc Natl Acad Sci USA* 99(26):16719–16724.
51. Pahlich S, Quero L, Roschitzki B, Leemann-Zakaryan RP, Gehring H (2009) Analysis of Ewing sarcoma (EWS)-binding proteins: Interaction with hnRNP M, U, and RNA-helicases p68/72 within protein-RNA complexes. *J Proteome Res* 8(10):4455–4465.
52. Paronetto MP, Miñana B, Valcárcel J (2011) The Ewing sarcoma protein regulates DNA damage-induced alternative splicing. *Mol Cell* 43(3):353–368.
53. Franceschini A, et al. (2013) STRING v9.1: Protein-protein interaction networks, with increased coverage and integration. *Nucleic Acids Res* 41(Database issue):D808–D815.
54. Park JH, et al. (2013) A multifunctional protein, EWS, is essential for early brown fat lineage determination. *Dev Cell* 26(4):393–404.
55. Paronetto MP, et al. (2014) Regulation of FAS exon definition and apoptosis by the Ewing sarcoma protein. *Cell Reports* 7(4):1211–1226.
56. Takahashi A, et al. (2003) EWS/ETS fusions activate telomerase in Ewing's tumors. *Cancer Res* 63(23):8338–8344.
57. Chai W, Ford LP, Lenertz L, Wright WE, Shay JW (2002) Human Ku70/80 associates physically with telomerase through interaction with hTERT. *J Biol Chem* 277(49): 47242–47247.
58. Wu XQ, et al. (2013) Feedback regulation of telomerase reverse transcriptase: New insight into the evolving field of telomerase in cancer. *Cell Signal* 25(12):2462–2468.
59. Wong MS, et al. (2013) Regulation of telomerase alternative splicing: A target for chemotherapy. *Cell Reports* 3(4):1028–1035.
60. Johansson FK, Göransson H, Westermark B (2005) Expression analysis of genes involved in brain tumor progression driven by retroviral insertional mutagenesis in mice. *Oncogene* 24(24):3896–3905.
61. Chen K, et al. (2008) CASP3 polymorphisms and risk of squamous cell carcinoma of the head and neck. *Clin Cancer Res* 14(19):6343–6349.
62. Aubol BE, et al. (2014) N-terminus of the protein kinase CLK1 induces SR protein hyperphosphorylation. *Biochem J* 462(1):143–152.
63. Ninomiya K, Kataoka N, Hagiwara M (2011) Stress-responsive maturation of Clk1/4 pre-mRNAs promotes phosphorylation of SR splicing factor. *J Cell Biol* 195(1):27–40.
64. Heidenblad M, et al. (2002) Detailed genomic mapping and expression analyses of 12p amplifications in pancreatic carcinomas reveal a 3.5-Mb target region for amplification. *Genes Chromosomes Cancer* 34(2):211–223.
65. Rozeman LB, et al. (2006) Array-comparative genomic hybridization of central chondrosarcoma: Identification of ribosomal protein S6 and cyclin-dependent kinase 4 as candidate target genes for genomic aberrations. *Cancer* 107(2):380–388.
66. Ye J, Renault VM, Jamet K, Gilson E (2014) Transcriptional outcome of telomere signalling. *Nat Rev Genet* 15(7):491–503.
67. Cao X, et al. (2014) The use of transformed IMR90 cell model to identify the potential extra-telomeric effects of hTERT in cell migration and DNA damage response. *BMC Biochem* 15:17.
68. Hisatomi H, et al. (2003) Expression profile of a gamma-deletion variant of the human telomerase reverse transcriptase gene. *Neoplasia* 5(3):193–197.
69. Duncan PI, Stojdl DF, Marius RM, Bell JC (1997) In vivo regulation of alternative pre-mRNA splicing by the Clk1 protein kinase. *Mol Cell Biol* 17(10):5996–6001.
70. Aubol BE, et al. (2013) Partitioning RS domain phosphorylation in an SR protein through the CLK and SRPK protein kinases. *J Mol Biol* 425(16):2894–2909.
71. Shi Y, Manley JL (2007) A complex signaling pathway regulates SRp38 phosphorylation and pre-mRNA splicing in response to heat shock. *Mol Cell* 28(1):79–90.
72. Zhang J, Bahi N, Llovera M, Comella JX, Sanchis D (2009) Polypyrimidine tract binding proteins (PTB) regulate the expression of apoptotic genes and susceptibility to caspase-dependent apoptosis in differentiating cardiomyocytes. *Cell Death Differ* 16(11): 1460–1468.
73. Wei Z, et al. (2011) Liprin-mediated large signaling complex organization revealed by the liprin-α/CASK and liprin-α/liprin-β complex structures. *Mol Cell* 43(4):586–598.
74. Ladenstein R, et al. (2010) Primary disseminated multifocal Ewing sarcoma: Results of the Euro-EWING 99 trial. *J Clin Oncol* 28(20):3284–3291.
75. Gorlick R, Janeway K, Lessnick S, Randall RL, Marina N; COG Bone Tumor Committee (2013) Children's Oncology Group's 2013 blueprint for research: Bone tumors. *Pediatr Blood Cancer* 60(6):1009–1015.
76. Le Deley MC, et al. (2010) Impact of EWS-ETS fusion type on disease progression in Ewing's sarcoma/peripheral primitive neuroectodermal tumor: Prospective results from the cooperative Euro-E.W.I.N.G. 99 trial. *J Clin Oncol* 28(12):1982–1988.
77. van Doorninck JA, et al. (2010) Current treatment protocols have eliminated the prognostic advantage of type 1 fusions in Ewing sarcoma: A report from the Children's Oncology Group. *J Clin Oncol* 28(12):1989–1994.
78. Schuck A, et al. (2003) Local therapy in localized Ewing tumors: Results of 1058 patients treated in the CESS 81, CESS 86, and EICESS 92 trials. *Int J Radiat Oncol Biol Phys* 55(1):168–177.
79. Womer RB, et al. (2012) Randomized controlled trial of interval-compressed chemotherapy for the treatment of localized Ewing sarcoma: A report from the Children's Oncology Group. *J Clin Oncol* 30(33):4148–4154.